www.czasopisma.pan.pl PAN www.journals.pan.pl
Chemical and Process Engineering 2021, 42 (4), 369–389
DOI: 10.24425/cpe.2021.138936

Effect of flow structure and colloidal forces on aggregation rate of small solid particles suspended in aqueous solutions

Grzegorz Tyl*[1], Juliusz Kondracki[2], Magdalena Jasińska[1]

[1]Faculty of Chemical and Process Engineering, Warsaw University of Technology, ul. Waryńskiego 1, 00-645 Warsaw, Poland
[2]Department of Applied Science and Technology, Politecnico di Torino, Corso Duca degli Abruzzi 24, 10129 Torino, Italy

In this paper aggregation of small solid particles in the perikinetic and orthokinetic regimes is considered. An aggregation kernel for colloidal particles is determined by solving the convection-diffusion equation for the pair probability function of the solid particles subject to simple shear and extensional flow patterns and DLVO potential field. Using the solution of the full model the applicability regions of simplified collision kernels from the literature are recognized and verified for a wide range of Péclet numbers. In the stable colloidal systems the assumption which considers only the flow pattern in a certain boundary layer around central particle results in a reasonable accuracy of the particle collision rate. However, when the influence of convective motion becomes more significant one should take into account the full flow field in a more rigorous manner and solve the convection-diffusion equation directly. Finally, the influence of flow pattern and process parameters on aggregation rate is discussed.

Keywords: aggregation, shear flow, DLVO, particles, colloidal forces, population balance

1. INTRODUCTION

Particulate products play a major role in today's industrial reality. In many applications the quality and properties of the final product depend on the fine structure and morphology of the dispersed solid phase. Particulate matter can be macroscopically characterized by particle size distribution (PSD) or specific area as well as in terms of their microstructure parameters like size of primary particles or fractal dimension of aggregates (Lazzari et al., 2016). All these properties can be crucial for product quality creating a need to understand the influence of process parameters on particulate matter characteristics like the size and morphology of particles. Mathematical modelling of processes carried out in multiphase systems still remains a challenge due to complex controlling mechanisms and dependence on many process parameters. The analysis of effective viscosity acting on the tracer particles of different size has been performed by Nicoud et al. (2015), showing variations of this parameter affected by considered length scale. The evolution

* Corresponding author, e-mail: grzegorz.tyl.dokt@pw.edu.pl

of dispersed phase systems can be described using population balance equations (PBEs) (Hulburt and Katz, 1964):

$$\frac{\partial f}{\partial t} + \sum_{i=1}^{3} \frac{\partial \left[v_i(\boldsymbol{x}, t) f \right]}{\partial x_i} + \sum_{j=1}^{N} \frac{\partial \left[G_j f \right]}{\partial r_j} = B(\boldsymbol{x}, \boldsymbol{r}, t) - D(\boldsymbol{x}, \boldsymbol{r}, t) \tag{1}$$

where f denotes the probability density function used to describe distribution of the dispersed phase properties, v_i, stands for the particle velocity in physical space characterized by coordinates x_i, G_j is the velocity of the particle in the internal space (i.e. dispersed phase properties), and finally B and D denote the birth and death functions, respectively used to describe aggregation or breakage processes. To predict the behaviour of the system one has to express B and D functions by applying kernels suitable for specific processes and process conditions. The kernel depends on the fluid properties, the flow pattern, and the particle properties.

In solid-liquid systems aggregation of particles remains the least understood phenomenon with many practical areas to develop. First papers considering aggregation in perikinetic and orthokinetic regimes date to the beginning of 20th century (Smoluchowski, 1916; Smoluchowski, 1917) laying the grounds for mathematical description of this phenomenon. Since then, there have been many attempts to develop collision kernels for perikinetic ($\mathrm{Pe} = \dfrac{Ea^2}{D^\infty} \ll 1$) (Fuchs, 1934; Spielman, 1970) and orthokinetic ($\mathrm{Pe} \gg 1$) (Camp and Stein, 1943; Saffman and Turner, 1956) regimes as well as for transitional zone described by moderate Péclet numbers (Melis et al., 1999; Swift and Friedlander, 1964; van de Ven and Mason, 1976; Zeichner and Schowalter, 1977). With the progress in fluid mechanics and colloid science these kernels have been supplemented including the effect of DLVO (Derjaguin and Landau, 1941; Verwey and Overbeek, 1948) interactions on aggregation rate as well as hydrodynamic effects due to fine scale motion of the carrier fluid. The above mentioned considerations allowed for better understanding of the influence of various process conditions on the aggregation of solid particles and provided a tool to describe this phenomenon quantitatively. The relative motion of two solid particles can be described by convection-diffusion equation for the pair probability function. It can be used to calculate collision rate of particles in a rigorous manner. Taking an ensemble average of convection-diffusion equation provides a platform to develop new, simplified collision kernels (Lattuada and Morbidelli, 2011; Zaccone et al., 2009). The work of Zaccone et al. (2009) was in fact the first paper presenting an analytical solution based on boundary-layer (matched asymptotics) analysis of the Smoluchowski convection-diffusion equation valid for solid particles subject to DLVO forces. Their theory provides, at least qualitatively, correct physical description and understanding of both fully numerical solutions as well as of experimental data (e.g. in terms of estimating lag-time for incipient coagulation/viscosity increase and of predicting bimodal cluster size distributions observed experimentally). These kernels are obviously much less computationally expensive and can be further used in population balance equations (PBEs) to simulate transient behaviour of the system under consideration.

In this paper mathematical modelling of the aggregation rate in nanoparticle colloidal systems subject to simple shear and extensional axisymmetric flow in laminar regime is considered. These conditions can also be met in turbulent flows, for boundary layers as well as for solid particles colliding at scales much smaller than the Kolmogorov microscale, η_k, satisfying the following condition:

$$a_i + a_j \ll \eta_k = \left(\frac{\nu^3}{\varepsilon} \right)^{1/4} \tag{2}$$

where a_i and a_j stand for the radii of two aggregating particles, ν being the kinematic viscosity of the fluid, and ε denoting the turbulent kinetic energy dissipation rate. A homogenous colloidal system in a dilute limit is considered i.e., only interactions of pair of equal sized, spherical particles are taken into account, neglecting the effects of inertia. In order to justify this assumption two characteristic timescales

can be compared i.e., the Kolmogorov timescale, τ_k, and the particle relaxation time, τ_r (Bałdyga and Krasiński, 2005):

$$\tau_k = \left(\frac{\nu}{\varepsilon}\right)^{1/2} \tag{3}$$

$$\tau_r = \frac{2}{9}\frac{a_i^2\left(\frac{\rho_s}{\rho_f}+\frac{1}{2}\right)}{\nu} \tag{4}$$

where ρ_s and ρ_f denote densities of a solid particle and a surrounding fluid, respectively. To omit the influence of inertia on the collision rate the condition $\tau_r \ll \tau_k$ must be satisfied leading to a following constraint:

$$a_i \ll \frac{3\sqrt{2}}{2}\left(\frac{\rho_s}{\rho_f}+\frac{1}{2}\right)^{-1/2}\eta_k \tag{5}$$

Holding to those assumptions the full convection-diffusion equation has been employed to analyse aggregation behaviour of colloidal particles with practical application to axisymmetric extensional flow describing flow conditions inside the smallest turbulent eddies (Batchelor and Green, 1972) as well as laminar shear flow characteristic for the near-wall region. The convection-diffusion equation has been solved after discretization with the finite differences allowing to compare the influence of the flow structure on aggregation rate. Similar approach has been used by Bal (2019, 2020) to study coagulation behaviour and stability regions of colloidal dispersions subject to shear flow and interaction forces (both DLVO and non-DLVO). In his work, however, another numerical technique, such as the finite element was used to solve convection-diffusion equation. Recently Banetta and Zaccone (2019) employed an intermediate asymptotics method to analytically solve convection-diffusion equation, which has been further used to study pair probability function profiles for colloidal systems subject to shear flow (Banetta and Zaccone, 2020). By comparison to rigorous solution, applicability regions of the simplified aggregation kernels can be recognized and verified, validating this way some of the assumptions made during development of models already published in subject literature.

2. THEORY

2.1. Convection-diffusion equation

In principle, the Eulerian description of an aggregation system is based on evaluating the field of pair probability function, c, around the central particle. Its evolution is governed by the convection-diffusion equation:

$$\frac{\partial}{\partial t}c\left(\vec{r},t\right) = \nabla\cdot\left(\overline{\overline{D}}\cdot\nabla c - \vec{v}_f\, c - \vec{v}_{\text{int}}\, c\right) \tag{6}$$

where $\overline{\overline{D}}$ is the Brownian diffusion tensor, $\vec{v}_f$ and $\vec{v}_{\text{int}}$ are the velocities of particles induced by fluid flow and interparticle forces respectively. The following boundary conditions are applied to obtain the solution:

$$c\left(|\vec{r}|\to\infty\right) = 1 \tag{7}$$

$$c\left(|\vec{r}| = 2a\right) = 0 \tag{8}$$

meaning that at infinite separation, $|\vec{r}|$, there is no disturbance to the particle concentration field and at $|\vec{r}| = 2a$ two particles collide.

Collision rate is then calculated by integrating the particle flux over the collision surface, S:

$$\beta = \int_S \left(\overline{\overline{D}}\cdot\nabla c - \vec{v}_f\, c - \vec{v}_{\text{int}}\, c\right)\cdot\vec{n}\,\mathrm{d}S \tag{9}$$

where $\vec{n}$ is the unit vector perpendicular to the infinitesimal surface element dS. It has to be indicated that in reaction rate limited aggregation Eq. (9) needs to be multiplied by collision efficiency to obtain aggregation rate constant for population balance application. Such expressions have been developed in the literature to include the effect of surface reaction (Bałdyga et al., 2019) or time required to build a solid bridge in case of microparticles (Bałdyga et al., 2004).

2.2. Brownian and convective motion of solid particles

The mutual diffusion coefficient of particles at infinite separation, D_{ij}^{∞}, can be expressed as a sum of diffusivities of two isolated particles (Smoluchowski, 1917):

$$D_{ij}^{\infty} = D_i^{\infty} + D_j^{\infty} = \frac{k_B T}{6\pi\mu}\left(\frac{1}{a_i} + \frac{1}{a_j}\right) \tag{10}$$

where k_B denotes the Boltzmann constant, T stands for the absolute temperature and μ is a dynamic viscosity of the fluid. When two particles encounter each other, Brownian diffusion is affected by the forces resulting from squeezing the liquid by two colliding particles (Batchelor, 1976). These effects can be introduced by applying two hydrodynamic functions, $G(r,\lambda)$ and $H(r,\lambda)$, which allows to predict damping of particle diffusion in radial and tangential directions, respectively. The diffusion tensor takes thus the following form, describing diffusion of particles in all considered directions:

$$\overline{\overline{D}} = D_{ij}^{\infty}\left[G(r,\lambda)\frac{\vec{r}\vec{r}}{r^2} + H(r,\lambda)\left(\overline{\overline{I}} - \frac{\vec{r}\vec{r}}{r^2}\right)\right] \tag{11}$$

where $r = |\vec{r}|$ is the interparticle distance, $\overline{\overline{I}}$ is a unit, second rank tensor, and $\lambda = a_j/a_i$.

Batchelor and Green (1972) proposed a general expression for a relative velocity of two particles subjected to fluid motion:

$$\vec{v}_f = \overline{\overline{E}}\cdot\vec{r} + \vec{\omega}\times\vec{r} - \left[A(r,\lambda)\frac{\vec{r}\vec{r}}{r^2} + B(r,\lambda)\left(\overline{\overline{I}} - \frac{\vec{r}\vec{r}}{r^2}\right)\right]\cdot\overline{\overline{E}}\cdot\vec{r} \tag{12}$$

with $\overline{\overline{E}} = \frac{1}{2}\left[\nabla\vec{u} + (\nabla\vec{u})^T\right]$ and $\vec{\omega} = \frac{1}{2}\nabla\times\vec{u}$ being the rate of strain tensor and angular velocity vector of the undisturbed velocity field, $\vec{u}$, of the fluid, whereas $A(r,\lambda)$ and $B(r,\lambda)$ represent hydrodynamic functions, which introduce the effects of presence of another particle in the vicinity of the considered one. Eq. (12) allows one to calculate the particle velocity for an arbitrary flow field, provided that it can be described by the rate of strain tensor and angular velocity vector. This work will focus on the comparison of two flow structures: an axisymmetric extensional, as well as a simple shear under laminar conditions of the flow regime.

In the latter case, we assume that the velocity component u_3 is linearly dependent on the x_2-direction, so the rate of strain tensor is expressed as follows:

$$\nabla\vec{u} = \begin{pmatrix} 0 & 0 & 0 \\ 0 & 0 & E_{23} \\ 0 & 0 & 0 \end{pmatrix} \tag{13}$$

where E_{23} is the shear rate. By applying it to Eq. (12) the following expressions for particle velocity components in spherical coordinates are obtained:

$$v_{f,r} = E_{23} r\,[1 - A(r,\lambda)]\sin^2\theta\sin\phi\cos\phi \tag{14}$$

$$v_{f,\theta} = E_{23} r\,[1 - B(r,\lambda)]\sin\theta\cos\theta\sin\phi\cos\phi \tag{15}$$

$$v_{f,\phi} = E_{23} r \sin\theta \left(\cos^2\phi - \frac{B(r,\lambda)}{2} \cos 2\phi \right) \tag{16}$$

Similarly, one can calculate the particle velocity field in the case of axisymmetric extensional flow described by the following rate of strain tensor:

$$\nabla \vec{u} = \begin{pmatrix} E_{11} & 0 & 0 \\ 0 & E_{22} & 0 \\ 0 & 0 & E_{33} \end{pmatrix} \tag{17}$$

where $E_{11} = E_{22} = -\frac{1}{2} E_{33}$ in order to satisfy the continuity equation. The velocity, $\vec{v}_f$, components in spherical coordinates are as follows:

$$v_{f,r} = \frac{1}{2} E_{33} r \left[1 - A(r,\lambda) \right] \left[3\cos^2\theta - 1 \right] \tag{18}$$

$$v_{f,\theta} = -\frac{3}{2} E_{33} r \left[1 - B(r,\lambda) \right] \sin\theta \cos\theta \tag{19}$$

The resulting velocity fields for $E_{23} = E_{33} = 2000\ \mathrm{s}^{-1}$ are presented in Fig. 1. When particle interactions are not present in the system under consideration solid particles just flow around the central one. Thus, even for particle trajectories very close to the central one aggregation will not occur due to lack of attractive forces.

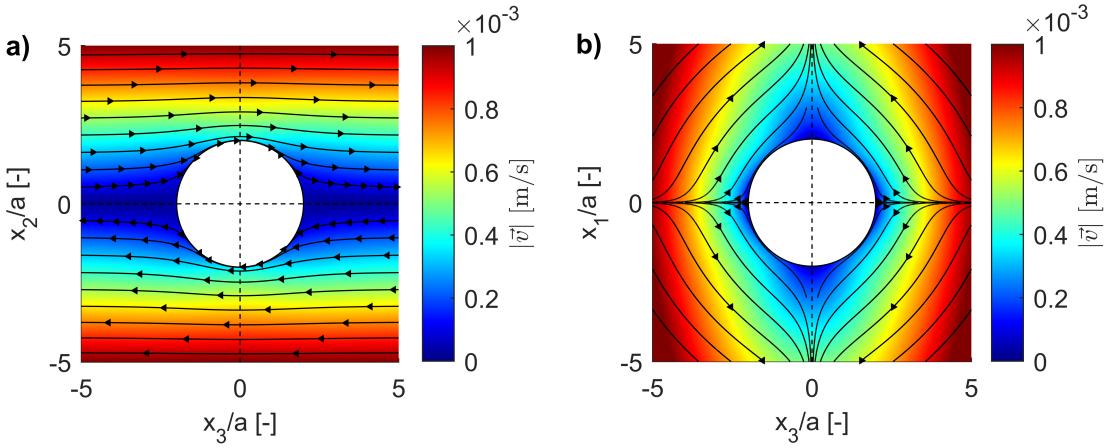

Fig. 1. Particle velocity fields in the vicinity of central particle with absence of interparticle interactions for a) simple shear flow, b) extensional flow pattern

2.3. Colloidal interactions

Small colloidal particles can interact with each other by both repulsive, V_R, and attractive, V_A, interparticle potentials. In what follows the DLVO theory (Derjaguin and Landau, 1941; Verwey and Overbeek, 1948) is used to describe these interactions, taking into account both the van der Waals and electrostatic forces due to the presence of an electric double layer formed in the vicinity of a given particle. Additionally, the superposition of attractive and repulsive potentials has been assumed in this approach.

The van der Waals potential energy between two particles can be described by the following relation, originally introduced by Hamaker (1937):

$$V_A = -\frac{A}{6} \left[\frac{2a_i a_j}{r^2 - (a_i + a_j)^2} + \frac{2a_i a_j}{r^2 - (a_i - a_j)^2} + \ln\left(\frac{r^2 - (a_i + a_j)^2}{r^2 - (a_i - a_j)^2} \right) \right] \tag{20}$$

where A denotes the particle's Hamaker constant.

The repulsive potential can be approximated by the formula proposed by Hogg et al. (1966):

$$V_R = \frac{\pi \epsilon a_i a_j}{a_i + a_j} \left(\Phi_i^2 + \Phi_j^2\right) \left\{ \frac{2\Phi_i \Phi_j}{\left(\Phi_i^2 + \Phi_j^2\right)} \ln \left[\frac{1 + \exp(-\kappa h)}{1 - \exp(-\kappa h)} \right] + \ln \left[1 - \exp(-2\kappa h)\right] \right\} \tag{21}$$

where Φ_i is the surface potential of particle i, $h = r - a_i - a_j$ denotes the surface-to-surface distance between two particles, and ϵ is the absolute permittivity. A Debye-Hückel constant, κ, is inversely proportional to the particle's double layer thickness and can be expressed as:

$$\kappa = \sqrt{2 \frac{e^2 I_s N_A}{\epsilon k_B T}} \tag{22}$$

where I_s is the ionic strength of the solution, N_A is the Avogadro number and e denotes an elementary charge. The relative velocity of particles induced by the colloidal interactions is then given by:

$$\vec{v}_{\text{int}} = -\frac{G(r, \lambda) D_{ij}^{\infty}}{k_B T} \nabla V \tag{23}$$

with total potential $V = V_A + V_R$. In what follows, a repulsion number, Rp, is used to characterize the system under consideration:

$$\text{Rp} = \frac{\epsilon \phi_i^2 a}{A} \tag{24}$$

with $a = \left(a_i + a_j\right)/2$. In Fig. 2 the scaled overall interaction potential is presented as a function of dimensionless interparticle distance, $\xi = r/a$, for several aggregating systems. As expected, larger values of Rp result in much higher potential barrier between particles, which in turn should lead to decrease in collision rates. Also, the reduction in electric double layer thickness causes the potential barrier to decline, which obviously should result in faster aggregation in the examined system. Please notice that for small repulsive forces (represented here by lower Rp value) the effect of the thickness of electric double layer is almost negligible as repulsive effects are completely damped. In case of large repulsive forces the effect of κ is however much more pronounced. Thus, increase of ionic strength can be one of the methods to enable aggregation in systems with large Rp values.

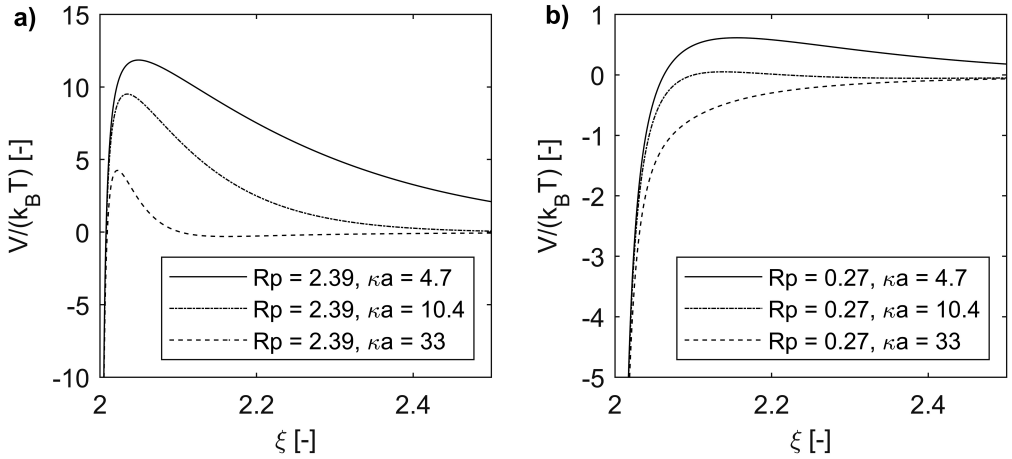

Fig. 2. Overall interparticle interaction potential for a) stable colloidal system, b) unstable colloidal system

As can also be observed in Fig. 2, the maximum of the barrier moves towards lower distances between particles which is directly linked with decrease of the thickness of electric double layer.

Additionally, the height of energy barrier is also decreased. Those two effects lead to an increased probability of interparticle collision. However, for the collision to be effective in forming of a stable aggregate another

step should be considered i.e., creation of an interparticle bond, which can be achieved either by surface reaction or formation of a bridge between particles by diffusion of surrounding material from the bulk of the solution. The second mechanism however is more relevant when larger particles are formed, due to higher stresses induced by the surrounding fluid. On the other hand, for large repulsion and large thickness of electric double layer particles are separated by larger distances and the probability of aggregation decreases to a greater extent.

In Figs. 3–5 the particle velocity fields are presented for both considered flow patterns and different system parameters. For the case of stable colloidal system, a clear influence of the interparticle repulsion can be noticed, bending the trajectories further away from the central particle. The pronounced deviation of the streamlines representing flow in the vicinity of central particle can be most clearly observed in Fig. 3a, which represents the case of a simple shear flow. In such systems decrease of the electric double layer thickness affects strongly the flow pattern surrounding the central particle; on the other hand, effective damping of the repulsive effects is visible in Fig 4a, where some trajectories pass very close to the considered particle. Finally, for the unstable colloidal system with negligible repulsion (Fig. 5a) trajectories for simple shear flow end up directly on the central particle leading eventually to physical bonding due to attractive van der Waals forces. Collision trajectories for axisymmetric extensional flow are shown in Figs. 3–5b. The effect of repulsion is not pronounced here in terms of streamlines. However, some sort of deviation in a very close vicinity of the considered particle for stable system is clearly observed in particular when a thin double layer is formed (Fig 3b).

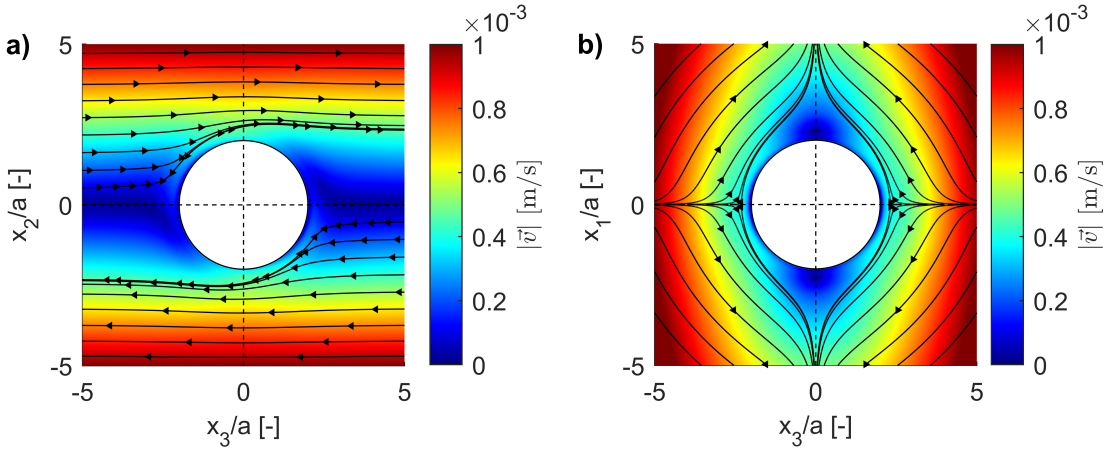

Fig. 3. Particle velocity fields in the vicinity of central particle for stable colloidal system (Rp = 2.39) with thick electric double layer (κa = 4.7) and a) simple shear flow, b) extensional flow pattern

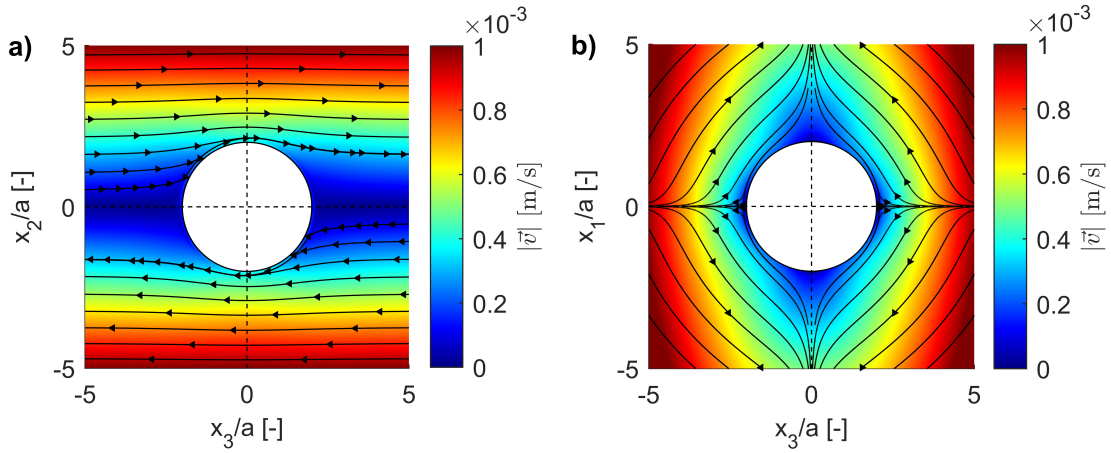

Fig. 4. Particle velocity fields in the vicinity of central particle for stable colloidal system (Rp = 2.39) with thin electric double layer (κa = 33) and a) simple shear flow, b) extensional flow pattern

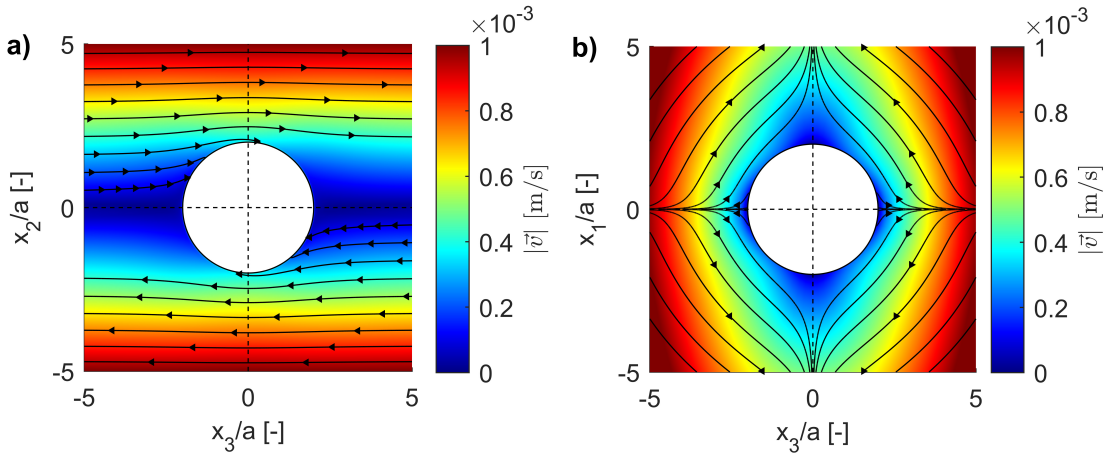

Fig. 5. Particle velocity fields in the vicinity of central particle for unstable colloidal system (Rp = 0.27) with thin electric double layer ($\kappa a = 33$) and a) simple shear flow, b) extensional flow pattern

3. NUMERICAL PROCEDURE

The full convection-diffusion equation, Eq. (6), has been solved after discretization using the finite differences. The aggregation rate can be then calculated by integrating the particle flux over the collision surface as follows:

$$\beta = \int_0^{2\pi}\int_0^{\pi}\left[r^2\left(v_{\mathrm{int},r}c + v_{f,r}c - D_r\frac{\partial c}{\partial r}\right)\right]_{r=a_i+a_j}\sin\theta\,\mathrm{d}\theta\,\mathrm{d}\phi \tag{25}$$

In case of extensional flow field, a numerical procedure described in detail in Melis et al. (1999) has been applied. Since velocity field is axisymmetric the mass flux in azimuthal direction can be omitted. Additionally, the diffusive flux in zenithal direction has been neglected since it is much smaller than the convective flux for most of the considered cases where Pe > 1. In cases where Pe < 1it has been shown (Zinchenko and Davis, 1994) that the diffusive flux in zenithal direction has only 2–3% impact on resulting collision rate. As a result, the full convection-diffusion equation (Eq. (6)) can be reduced to a two-dimensional case:

$$\frac{1}{r^2}\frac{\partial}{\partial r}\left[r^2\left(v_{\mathrm{int},r}c + v_{f,r}c - D_r\frac{\partial c}{\partial r}\right)\right] + \frac{1}{r\sin\theta}\frac{\partial}{\partial\theta}\left(\sin\theta v_{f,\theta}c\right) = 0 \tag{26}$$

As a first step Eq. (27) is solved for $\theta = \dfrac{\pi}{2}$. In this case the velocity in zenithal direction, $v_{f,\theta}$, vanishes bringing Eq. (27) to a second order ordinary differential equation:

$$\frac{1}{r^2}\frac{\mathrm{d}}{\mathrm{d}r}\left\{r^2\left[\left(v_{\mathrm{int},r} - \frac{E_{33}}{2}(1-A)r\right)c - D_r\frac{\partial c}{\partial r}\right]\right\} + \frac{3}{2}E_{33}(1-B)c = 0 \tag{27}$$

which has been further discretized using finite differences and solved after applying boundary conditions given by Eqs. (7) and (8). The far field boundary condition has been implied assuming $r = 30a$. Solution of Eq. (28) serves then as a starting point for the integration of Eq. (21) in zenithal direction. Due to the limitations in size of computational domain it is not possible to implement a far field boundary condition (Eq. (7)) on the whole domain boundary. To overcome this issue, an *upstream* and a *downstream* regions have been distinguished in the computational domain, separated by the critical angle, $\theta_{\mathrm{cr}} = \arccos\dfrac{1}{\sqrt{3}}$, where the radial velocity component vanishes. In the *upstream* region a far field boundary condition (Eq. (7)) has been imposed. In the *downstream* region however an open boundary condition, $\dfrac{\partial c}{\partial r} = 0$, has been used. The schematic representation of the computational domain for this case has been presented in Fig. 6.

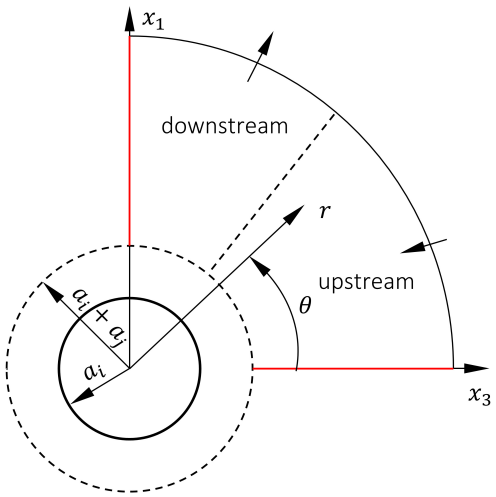

Fig. 6. Schematic representation of computational domain for $\theta = \pi/2$ symmetry plane and extensional flow

For the case of simple shear flow the problem cannot be reduced to two dimensions since the flow field is not axisymmetric. Following considerations of van de Ven and Mason (1976), the diffusive flux in zenithal direction has been omitted as well as the steady state assumed, the same way as in the case of an extensional flow, neglecting as a result the first r.h.s. term, $\frac{\partial c}{\partial t}$, of Eq. (6). However, the mass flux in the azimuthal direction cannot be neglected. The above mentioned assumptions lead to Eq. (6) in the form:

$$\frac{1}{r^2}\frac{\partial}{\partial r}\left[r^2\left(v_{\mathrm{int},r}c + v_{f,r}c - D_r\frac{\partial c}{\partial r}\right)\right] + \frac{1}{r\sin\theta}\frac{\partial}{\partial\theta}\left(\sin\theta v_{f,\theta}c\right) + \frac{1}{r\sin\theta}\frac{\partial}{\partial\phi}\left[v_{f,\phi}c - \frac{1}{r}D_\phi\frac{\partial c}{\partial\phi}\right] = 0 \quad (28)$$

Although the problem is more complex from the numerical point of view than in the previous case, still some more simplifications can be made. First, the size of computational domain has been reduced by applying the symmetry boundary condition on the $\theta = \frac{\pi}{2}$ plane. Secondly, it can be noticed that the solution is periodic i.e., $c(r,\theta,\phi) = c(r,\theta,\phi+\pi)$.

The solution procedure starts with solution of Eq. (28) on the boundaries of computational domain i.e., $\theta = 0$ and $\theta = \frac{\pi}{2}$. In the first case, for $\theta = 0$, convection flux terms vanish reducing Eq. (28) to the following ordinary differential equation:

$$\frac{1}{r^2}\frac{\mathrm{d}}{\mathrm{d}r}\left[r^2\left(D_r\frac{\mathrm{d}c}{\mathrm{d}r} - v_{\mathrm{int},r}c\right)\right] = 0 \quad (29)$$

Likewise, in the case of $\theta = \frac{\pi}{2}$, $v_{f,\theta}$ vanishes, and Eq. (28) simplifies to the following two-dimensional PDE:

$$\frac{1}{r^2}\frac{\partial}{\partial r}\left[r^2\left(D_r\frac{\partial c}{\partial r} - v_{\mathrm{int},r}c - v_{f,r}c\right)\right] - \frac{1}{r}\frac{\partial}{\partial\phi}\left(v_{f,\phi}c - \frac{1}{r}D_\phi\frac{\partial c}{\partial\phi}\right) + \frac{1}{r}E_{23}(1-B)\sin\phi\cos\phi = 0 \quad (30)$$

Both Eq. (29) and Eq. (30) were discretized by approximating spatial derivatives with central finite differences and the resulting system of linear equations was solved using the *mldivide* utility in MATLAB R2020b. To implement the $c(r\to\infty) = 1$ boundary condition, similarly as in the case of extensional flow pattern, two regions of computational domain have been distinguished namely, *upstream* and *downstream* (see Fig. 7). In the upstream region the radial component of the velocity vector, $\vec{v}_f$, is negative, so the vector is pointing towards the central particle, while in the downstream region, this component is positive and the vector points outwards. It can be shown that $v_{f,r} = 0$ for $\phi = 0$ determining the upstream region for $-\frac{\pi}{2} < \phi \le 0$ and the downstream region for $0 < \phi \le \frac{\pi}{2}$. Thus, $c = 1$ is imposed at the outer boundary of the upstream region and $\frac{\partial c}{\partial r} = 0$ at the outer boundary of the downstream region.

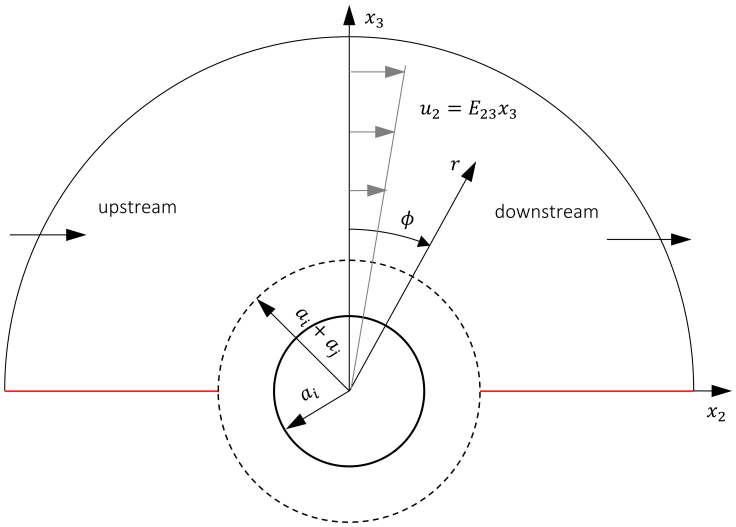

Fig. 7. Schematic representation of computational domain for $\theta = \pi/2$ symmetry plane and simple shear flow pattern

After solving Eqs. (29) and (30) with proper boundary conditions it was also possible to calculate the global solution. For this purpose, Eq. (28) has been also discretized by approximating derivatives with central finite differences and the resulting system of linear equations was solved using the *mldivide* MATLAB function.

In presented simulations the computational domain has been limited to $2a \leq r \leq 25a$. The spatial grid size in the r-direction was set to $\Delta r_1 = 0.0025a$ for $r \leq 3a$, where high concentration gradients are expected, and $\Delta r_2 = 0.0733a$ for $3a < r \leq 25a$. In zenithal and azimuthal directions spatial grid sizes equal to $\Delta\phi = 0.0052$ and $\Delta\theta = 0.0524$ respectively have been used.

4. SIMPLIFIED AGGREGATION KERNELS

Several robust and less computationally expensive collision kernels intended to work for a wide range of Péclet numbers have been presented in the past two decades (Bałdyga and Orciuch, 2001; Lattuada and Morbidelli, 2011; Zaccone et al., 2009). This work will focus on the first two of them since they have been developed for extensional as well as simple shear flow patterns. They have been derived from an ensemble averaged convection-diffusion equation in the form:

$$\frac{1}{r^2}\frac{\partial}{\partial r}\left[r^2\left(v_{\mathrm{int},r}\bar{c} + \overline{v_{f,r}c} - D_r\frac{\partial \bar{c}}{\partial r}\right)\right] = 0 \tag{31}$$

The first considered kernel from this family, proposed by Zaccone et. al. (2009) was developed by introducing the concepts of the effective velocity profile, $\bar{v}_{f,r}$. This assumption should be valid for low to moderate values of extension/shear rates. Eq. (31) has been solved only inside the boundary layer to allow for the solution to converge in a far field boundary which was imposed for $\xi = 2 + \delta$. As a result, an expression for aggregation rate has been obtained:

$$\beta_{\mathrm{agg}} = \frac{4\pi D_{ij}^{\infty}\left(a_i + a_j\right)}{2\int\limits_{2}^{2+\delta}\dfrac{\exp\left(\int\limits_{2+\delta}^{\xi}\left(-\mathrm{Pe}\cdot f(\xi) + \frac{\mathrm{d}V}{\mathrm{d}\xi}\right)\mathrm{d}\xi\right)}{G(\xi,\lambda)\xi^2}\mathrm{d}\xi} \tag{32}$$

where $\xi = \dfrac{2r}{a_i + a_j}$ denotes the dimensionless distance between two particles, $\delta = c_2\sqrt{\dfrac{2}{\mathrm{Pe}\cdot\kappa\left(a_i + a_j\right)}}$ is the boundary layer thickness with c_2 being a prefactor having an order of magnitude equal to 1, $f(\xi)$ is the effective velocity profile which for the case of axisymmetric extensional flow takes the form $f(\xi) = -\dfrac{\xi\left(1 - A(r,\lambda)\right)}{3\sqrt{3}G(r,\lambda)}$ and $f(\xi) = -\dfrac{\xi\left(1 - A(r,\lambda)\right)}{3\pi G(r,\lambda)}$ for the simple shear flow.

A modified version of the model presented by Zaccone at. al. (2009) was proposed by Lattuada and Morbidelli (2011). To impose a far field boundary condition for $\xi \to \infty$, Eq. (31) has been solved in a rigorous way inside a boundary layer as in the previously considered kernel. Outside boundary layer interparticle interactions have been neglected, and an unrealistic velocity profile $f(\xi) = -\dfrac{1}{\xi^2}$ has been used leading to:

$$\beta_{\mathrm{agg}} = \frac{4\pi D_{ij}^{\infty}\left(a_i + a_j\right)}{2\int\limits_2^{\infty} \dfrac{\exp\left(\mathrm{He}(2+\delta-\xi)\left(\int\limits_{2+\delta}^{\xi}\left(-\mathrm{Pe}\cdot f(\xi) + \frac{\mathrm{d}V}{\mathrm{d}\xi}\right)\mathrm{d}\xi - \mathrm{Pe}\frac{\alpha}{2+\delta}\right) - \mathrm{Pe}\cdot\mathrm{He}(\xi-2-\delta)\frac{\alpha}{\xi}\right)}{G(\xi,\lambda)\xi^2}\mathrm{d}\xi} \tag{33}$$

where He is the Heaviside step function. In the model there are two adjustable parameters: c_2 in the definition of boundary layer thickness and α, which is required to grasp the size dependence of aggregation rate for high Pe values. The set of constants used for the simulations as well as the method of their estimation has been briefly presented in the Appendix. A more detailed description of the estimation method for model parameters has been provided as the supplementary material to the original paper (Lattuada and Morbidelli, 2011). It has to be noted that the assumed velocity profile outside the considered boundary layer is unphysical. The main reason for this assumption was to obtain an expression for coagulation rate in a closed form without significant errors in the resulting values. However, due to the presence of the two free model parameters allowing one to tune the model to the system under consideration it is not recommended to use it as a predictive tool for description of aggregating systems.

5. RESULTS AND DISCUSSION

In what follows, the aggregation of equal size polystyrene (Ha $= \dfrac{A}{k_B T} = 1.58$) particles suspended in aqueous continuous phase has been considered. However, the presented approach can be applied also to model heteroaggregation. The solution of Eq. (6) provides a profile of the pair probability function, c, around the central particle, which can be regarded as a concentration of other particles in the vicinity of the considered one.

In Figs. 8–10 examples of pair probability function profiles are presented for both simple shear and extensional flow patterns in case of unstable (Fig. 8) and stable (Figs. 9, 10) colloidal systems assuming the same rates of shear and elongation equal to $E_{23} = E_{33} = 2000\ \mathrm{s}^{-1}$, respectively. In the case of stable colloidal system, the influence of electric double layer thickness on pair probability function profile has been also presented.

It can be noticed that the flow structure of surrounding fluid has a significant effect on the pair probability function profile including local gradients which determine the mass flux at collision surface, and hence the rate of aggregation. Additionally, an overshoot of c profiles ($c > 1$) can be clearly observed for presented conditions in the stable colloidal system, close to the collision surface. It means that due to interparticle repulsion, particles in those regions move slower than surrounding fluid causing the solid

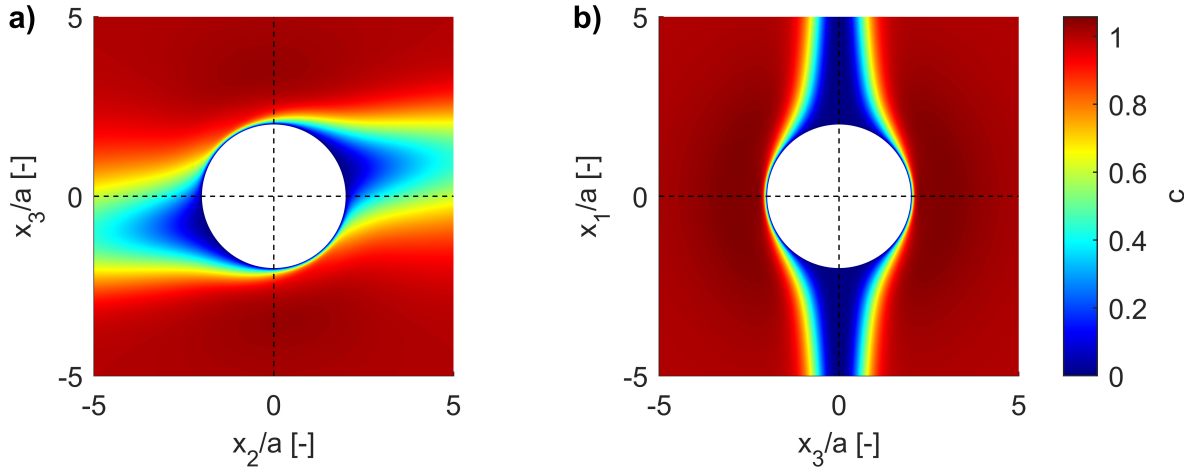

Fig. 8. Pair probability function profile around the collision surface for unstable colloidal system (Rp = 0.27, $\kappa a = 33$) and a) simple shear flow on $\theta = \pi/2$ symmetry plane, b) axisymmetric extensional flow

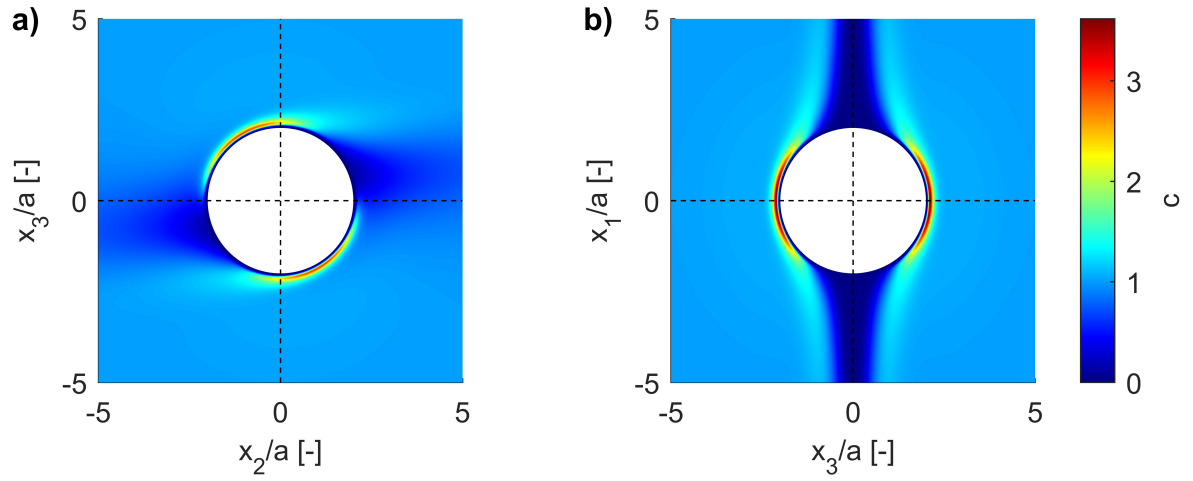

Fig. 9. Pair probability function profile around the collision surface for stable colloidal system (Rp = 2.39) with thin electric double layer ($\kappa a = 33$) for a) simple shear flow on $\theta = \pi/2$ symmetry plane, b) axisymmetric extensional flow

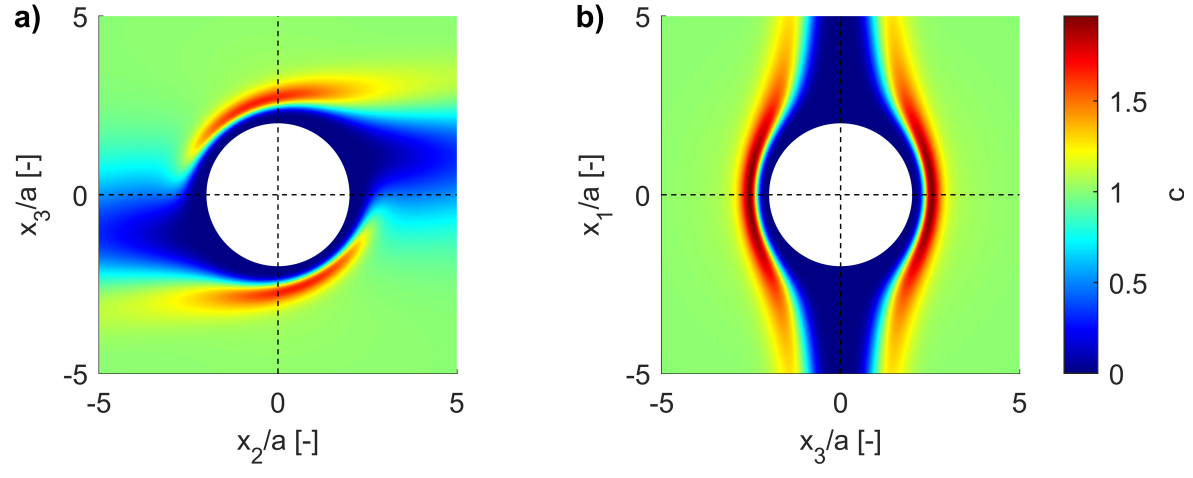

Fig. 10. Pair probability function profile around the collision surface for stable colloidal system (Rp = 2.39) with thick electric double layer ($\kappa a = 4.7$) for a) simple shear flow on $\theta = \pi/2$ symmetry plane, b) axisymmetric extensional flow

phase concentration to increase. The maximum value of the pair probability function in the "overshoot" region is higher for the case with thin electric double layer resulting in higher concentration gradients, and hence resulting in faster aggregation. Calculated pair probability function profiles can be further used to determine collision rate with application of Eq. (9).

In Fig. 11b the effect of particle size on aggregation rate is presented for the system with thick electric double layer ($\mathrm{Rp}/a = 2.39{\cdot}10^7$ m^{-1}, $\kappa = 1.04{\cdot}10^8$ m^{-1}) for different shear/extension rates. For the case of no shear or elongation the predicted aggregation rate constant decreases monotonously with the size of colliding particles due to decrease of their relative diffusivity and increasing impact of repulsive forces. However, in case of high shear/extension rates a minimum value of aggregation rate occurs when the convective motion becomes dominant. Please also notice that location of this minimum depends on flow structure and apparently location of the minimum moves towards smaller sizes in case of the extensional flow. This is due to change in particle transport mechanism from diffusion to convection. According to the equation for Brownian diffusion (Eq. (10)) the larger the particles the lower the diffusion coefficient and thus in Fig. 11 the decrease of aggregation rate can be clearly observed for smaller sizes. On the contrary, in the region of larger particles the convective flux ($u{\cdot}c$) starts to dominate over diffusive flux ($D_r \dfrac{\mathrm{d}c}{\mathrm{d}r}$) and the increase in aggregation rates prevails. This behaviour is however limited only to the larger values of shear/extension rates. For lower values of shear/extension only a sort of deviation from linear behaviour characteristic for diffusional regime can be noticed. For the system with a thin electric double layer ($\mathrm{Rp}/a = 4.25{\cdot}10^7$ m^{-1}, $\kappa = 4.4{\cdot}10^8$ m^{-1}) presented in Fig. 11a, the influence of convection is much weaker, with no minimum aggregation rate value predicted for considered shear/extension rates.

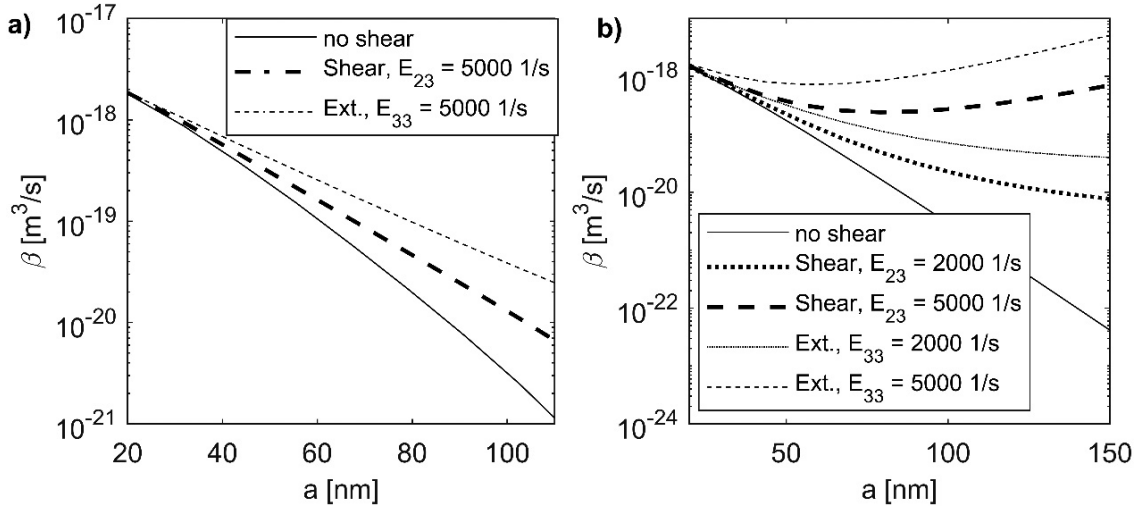

Fig. 11. Dependence of aggregation rate on particle size for a) thin electric double layer, b) thick electric double layer

Let us now present a comparison of direct impact of flow structure on aggregation rate. To do this, the effect of an average energy dissipation needs to be introduced. The method of its determination is specific for the flow type i.e. axisymmetric extensional or shear flow, as considered in the present work. The average energy dissipation rate is given by:

$$\varepsilon = 2\nu E_{ij} E_{ij} \tag{34}$$

Substituting now appropriate components of the strain rate tensor defined either by Eq. (13) or Eq. (17) for the shear and extensional flow respectively, one can simply relate an average energy dissipation rate with the corresponding values of shear and extension rates:

$$\varepsilon = \nu E_{23}^2 \tag{35}$$

applicable for simple shear flow, and

$$\varepsilon = 3\nu E_{33}^2 \tag{36}$$

applicable for extensional flow.

In Fig. 12 the predicted aggregation rate constants have been presented for unstable (Rp = 0.27) and stable (Rp = 2.39) colloidal systems respectively, for both types of flow structure and for different electric double layer thickness characterized by value of κa.

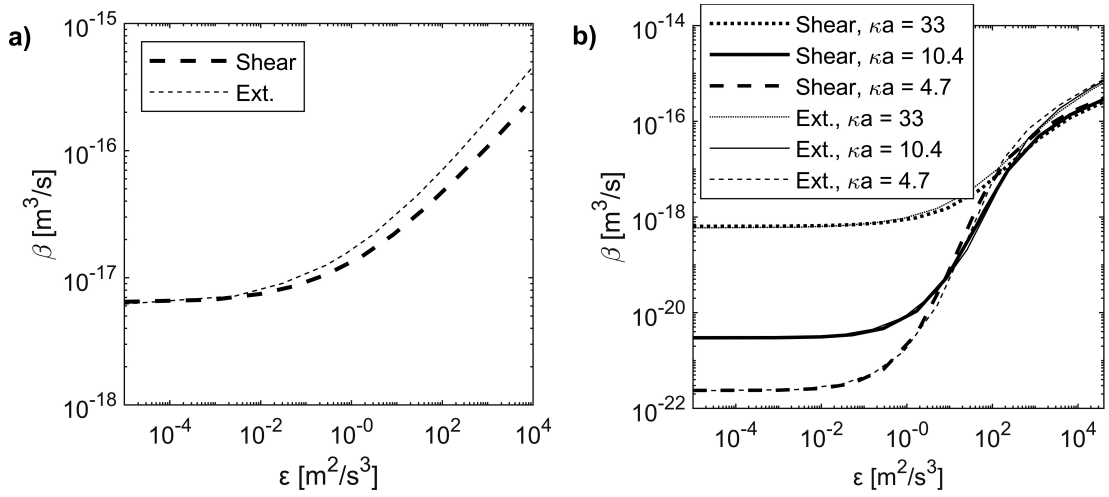

Fig. 12. Aggregation rate constant for a) unstable colloidal system (Rp = 0.27), b) stable colloidal system (Rp = 2.39)

For low values of average energy dissipation rate in the system collision rate reaches the perikinetic limit which is governed by Brownian motion with a clear influence of interparticle interactions given by Eq. (21) and Eq. (22). This asymptotic value can be determined using classical perikinetic kernel of Smoluchowski (1916) divided by the Fuchs stability ratio (Fuchs, 1934), in the form presented by Spielman (1970):

$$\beta_{\text{agg}} = \frac{4\pi D_{ij}^{\infty}\left(a_i + a_j\right)}{W} \tag{37}$$

$$W = 2\int_2^{\infty} \frac{\exp\left(\dfrac{V}{k_B T}\right)}{G(\xi,\lambda)\xi^2}\,\mathrm{d}\xi \tag{38}$$

In the case of thin electric double layer (high values of κa) aggregation rate in the perikinetic limit is higher than that for thick electric double layer due to weaker repulsion forces. With increasing average energy dissipation rate this difference gradually decreases leading to an asymptotic orthokinetic limit, where the convective effects become dominant. Here, aggregation rate is proportional to $\beta_{\text{agg}} \sim E_{23}^{0.77}$ for shear flow and $\beta_{\text{agg}} \sim E_{33}^{0.86}$ for extensional flow (Zeichner and Schowalter, 1977), with negligible effect of Brownian diffusion and interparticle forces. In the case of extensional flow, collision rate of particles is higher than for shear flow, for the given average energy dissipation rate in the system. It means that aggregation in shear flow pattern is less energetically effective than in axisymmetric extensional flow. This effect however becomes significant only for moderate to high values of ε.

To simulate behaviour of aggregating systems using CFD codes one needs to define aggregation kernel in a reasonably simple form, which would not require long computational times. Such expressions for a wide range of Péclet numbers can be developed based on the averaged convection-diffusion equation. Aggregation kernels valid for two flow patterns considered in the present work have been developed by Zaccone et al. (2009) and further extended by Lattuada and Morbidelli (2011). In Figs. 13, 14 and 15

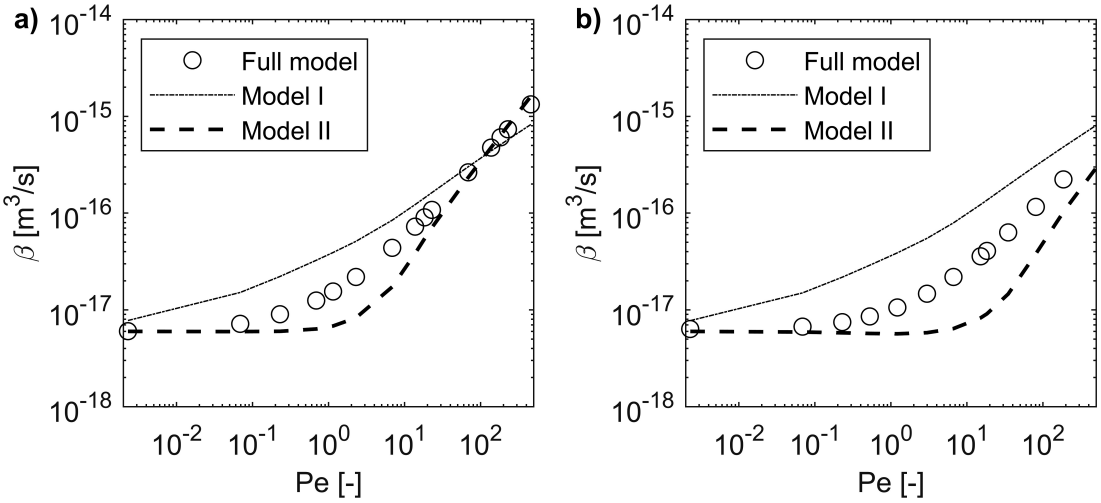

Fig. 13. Aggregation rate for unstable colloidal system (Rp = 0.27) and a) extensional, b) simple shear flow (Model I – Zaccone et al. (2009); Model II – Lattuada and Morbidelli (2011))

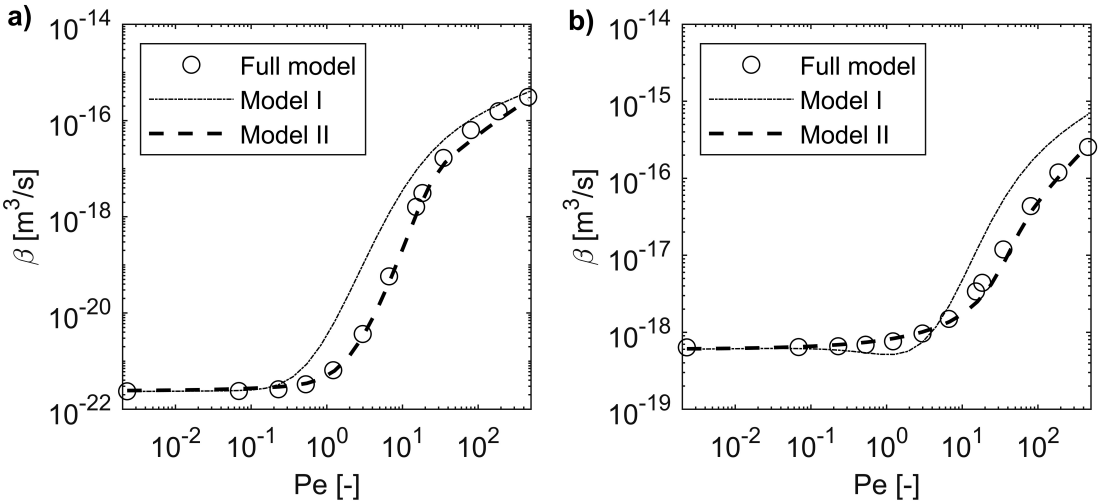

Fig. 14. Aggregation rate for simple shear flow and stable colloidal system (Rp = 2.39) with a) thick (κa = 4.7) and b) thin (κa = 33) double layer (Model I – Zaccone et al. (2009); Model II – Lattuada and Morbidelli (2011))

their predictions are compared to the results obtained by direct solution of convection-diffusion equation presented in detail in this paper and addressed in Figures as "full model".

In all the considered cases, for low Péclet numbers both simplified models reach the perikinetic limit reasonably well provided that the stable colloidal system is considered. In the unstable case however Model I gives the same values of aggregation rates in perikinetic limit only for Pe number as low as 10^{-3}. For moderate values of Pe predictions of both Model I and II differ from the full solution. It is also worth noticing that Model I overestimates β values while Model II underestimates them for the considered values of model parameters. A clear deviation from full approach is more pronounced in case of simple shear flow as can be easily noticed by comparison of results presented in Figs. 13a and 13b. Moreover, for the case of unstable colloidal system, the kernel by Zaccone et al. (2009) does not predict the plateau in low shear conditions which is, on the other hand, clearly predicted by simulation with the full model. For the case of stable colloidal system (Figs. 14 and 15) Model I generally overestimates the collision rate except for the axisymmetric extensional flow and thin electric double layer, where predicted values fit quite well. On the other hand, Model II reproduces collision rates very well for both flow structures provided that colloidal system is stable.

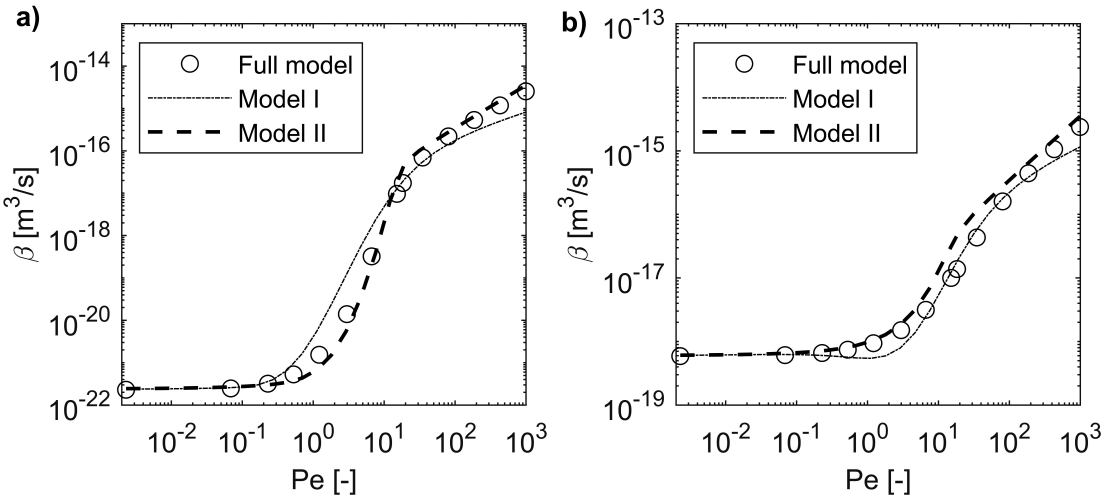

Fig. 15. Aggregation rate for axisymmetric extensional flow and stable colloidal system (Rp = 2.39) with a) thick (κa = 4.7) and b) thin (κa = 33) double layer (Model I – Zaccone et al. (2009); Model II – Lattuada and Morbidelli (2011))

All these observations lead to a simple conclusion that the presented model (Model I) is limited to the very narrow examples of stable colloidal systems mostly in the range of perikinetic limit. It is also not recommended to use it in case of aggregation in a simple shear flow, especially when the effect of convective transport becomes important. As for the case of extensional flow, comparison looks reasonably well only for the stable colloidal systems with the thin double layer. Model I also should not be applied either for moderate Pe number (overpredicts) or very high Pe number (underpredicts) in case of stable thick double layer system.

The modified kernel by Lattuada and Morbidelli (2011) reproduces collision rates more precisely for all stable colloidal systems considered, showing that inclusion only of the boundary layer flow pattern as done by Zaccone et al. (2009) is not sufficient to properly represent such a system in many cases. It seems also that both considered simplified models are unable to predict properly shear/extension rate dependence in the asymptotic orthokinetic limit. Especially in the case of unstable colloidal systems, prediction of simplified kernels differ significantly from the results obtained by solving the full model. In such cases the realistic velocity fields should be used for the solution, since the assumptions made during model development in the simplified approaches introduce significant errors. To predict aggregation rates in the high energy dissipation regions the full approach should be applied or another improvement to the method of closure proposed. This is going to be the subject of the further model development which authors of the present paper would like to focus on in the nearest future. Determination of aggregation kernel for high Péclet number can be practically important in case of seeking for equilibrium formation between breakage and collision of particles of any sizes and internal structures subject to real flow systems with high energies.

6. CONCLUSIONS

In this work aggregation of small solid particles has been considered. The convection-diffusion equation has been solved using finite differences method to obtain the profiles of pair probability function around the central particle. These profiles have been further used to calculate aggregation kernel for simple shear and axisymmetric flow patterns, as well as to examine the effect of a range of process and system parameters, including size of aggregating particles and average energy dissipation rate. Influence of DLVO forces on

aggregation rate has been shown by considering stable and unstable colloidal systems with a thin and thick electric double layer, which can be affected simply by changing the ionic strength of the solution. All those parameters affect the distribution of pair probability function as well as its local gradients which constitute the driving force for aggregation. Results obtained by solving the full convection-diffusion equation allow to predict the system behaviour for a wide range of Péclet number values, starting from the perikinetic limit characterized by kernel of Smoluchowski (1916) divided by the stability ratio (Fuchs, 1934) up to orthokinetic asymptotic limits described by Zeichner and Schowalter (1977). Results presented in this work are also in agreement with data published by Bal (2020) for simple shear flow solved with the application of the finite element method. However, at least for the set of process parameters used in the present work, the coagulation rate minimum for intermediate shear rate has not been spotted and thus cannot be confirmed. Additionally, the results obtained here do not agree with the findings of Bal (2020) that electric double layer repulsion remains significant for high shear rates leading to orthokinetic limit dependent on repulsion force strength and double layer thickness. For all of the cases considered in the current paper, the orthokinetic limits were in agreement with those described in Zeichner and Schowalter (1977) i.e. to $\beta_{\text{agg}} \sim E_{23}^{0.77}$ and $\beta_{\text{agg}} \sim E_{33}^{0.86}$ for shear and extensional flow fields respectively.

Finally, predictions of the simplified aggregation kernels have been validated against the solution of the full model. For stable colloidal systems both considered models gave precise representation of aggregation rate in perikinetic limit for the considered set of model parameters. It shows that considering only a certain boundary layer around the central particle as was done by Zaccone et al. (2009) is enough to characterize such systems. For moderate Péclet numbers, the model shows that the flow field further away from the central particle starts to affect the behaviour of the system and it needs to be considered as well. For the cases of stable colloid systems presented in this work including the velocity field outside the boundary layer even in an unrealistic form, as was done by Lattuada and Morbidelli (2011), it leads to significant improvement of the model behaviour. In the case of unstable colloidal system, where the impact of flow is the strongest, both simplified approaches (Models I and II) show major divergence from the solution of the full convection-diffusion equation. In the systems so strongly dependent on convective motion the velocity field around the central particle should be considered in a rigorous manner to obtain a precise solution. Being aware of the limitations of simplified approaches in predicting aggregation rate, they can provide an approximate characterization of the system with reasonable execution time, being the key issue for further implementation in CFD codes. Thus, the presented models should be further developed and extended to simulate collisions of nanoparticles in turbulent flow in case of boundary layer forming close to the system walls as well as for the flow field encountered inside the smallest turbulent eddies.

SYMBOLS

a	particle radius, m
A	Hamaker constant, J
$A(r,\lambda)$	hydrodynamic function
$B(r,\lambda)$	hydrodynamic function
$B(\boldsymbol{x},\boldsymbol{r},t)$	birth function, $\text{m}^{-4}\text{s}^{-1}$
c	pair probability function
$\overline{\overline{D}}$	diffusion tensor, m^2s^{-1}
$D(\boldsymbol{x},\boldsymbol{r},t)$	death function, $\text{m}^{-4}\text{s}^{-1}$
e	elementary charge, C
$\overline{\overline{E}}$	rate of strain tensor, s^{-1}
f	number density function, m^{-4}
G	growth rate, m/s
$G(r,\lambda)$	hydrodynamic function

h	distance between surfaces of colliding particles, m
$H(r, \lambda)$	hydrodynamic function
Ha	dimensionless Hamaker constant
I_S	ionic strength, mol/dm^3
k_B	Boltzmann constant, J/K
N_A	Avogadro number, mol^{-1}
Pe	Péclet number
r	interparticle distance, m
$\boldsymbol{r}$	position in phase space
Rp	repulsion number
S	surface area, m^2
t	time, s
T	absolute temperature, K
u	undisturbed fluid velocity, m/s
v	particle velocity, m/s
V	interaction potential, J
$\boldsymbol{x}$	position in physical space, m

Greek symbols

β	particle collision rate, m^3/s
δ	boundary layer thickness, m
ε	average energy dissipation rate, m^2/s^3
ϵ	electric permittivity, F/m
η_k	Kolmogorov length microscale, m
θ	position in zenithal direction, rad
κ	inverse of Debye length, m^{-1}
λ	ratio of particles' radii
μ	dynamic viscosity, Pa·s
ν	kinematic viscosity, m^{2}s^{-1}
ξ	dimensionless interparticle distance
ρ	density, kg/m^3
τ_k	Kolmogorov time microscale, s
τ_r	particle relaxation time, s
ϕ	position in azimuthal direction, rad
Φ	particle surface potential, V
ω	angular velocity, rad/s

Superscripts

A	attractive
cr	critical
f	fluid
i, j	particle indices
int	interaction
r	radial
R	repulsive
s	solid
ϕ	azimuthal
θ	zenithal

Subscripts

∞	isolated particle

ACKNOWLEDGEMENTS

This work was financially supported by the Polish National Science Centre (Grant agreement number: UMO-2017/27/B/ST8/01323).

REFERENCES

Bal V., 2019. Stability characteristics of nanoparticles in a laminar linear shear flow in the presence of DLVO and non-DLVO forces. *Langmuir*, 35, 11175–11187. DOI: 10.1021/acs.langmuir.9b01886.

Bal V., 2020. Coagulation behavior of spherical particles embedded in laminar shear flow in presence of DLVO and non-DLVO forces. *J. Colloid Interface Sci.*, 564, 170–181. DOI: 10.1016/j.jcis.2019.12.119.

Bałdyga J., Jasińska M., Krasiński A., Rożeń A., 2004. Effects of fine scale turbulent flow and mixing in agglomerative precipitation. *Chem. Eng. Technol.*, 27, 315–323. DOI: 10.1002/ceat.200401993.

Bałdyga J., Krasiński A., 2005. Precipitation of benzoic acid in continuous stirred tank – effects of agglomeration, In: Ulrich J. (Ed.), *Proceedings of 16th International Symposium on Industrial Crystallization*. VDI-Verlag, 411–416.

Bałdyga J., Orciuch W., 2001. Some hydrodynamic aspects of precipitation. *Powder Technol.*, 121, 9–19. DOI: 10.1016/S0032-5910(01)00368-0.

Bałdyga J., Tyl G., Bouaifi M., 2019. Aggregation efficiency of amorphous silica nanoparticles. *Chem. Eng. Technol.*, 42, 1717–1724. DOI: 10.1002/ceat.201900091.

Banetta L., Zaccone A., 2019. Radial distribution function of Lenard-Jones fluids in shear flow from intermediate asymptotics. *Phys. Rev. E*, 99, 052606. DOI: 10.1103/PhysRevE.99.052606.

Banetta L., Zaccone A., 2020. Pair correlation function of charge-stabilized colloidal systems under sheared conditions. *Colloid Polym. Sci.*, 298, 761–771. DOI: 10.1007/s00396-020-04609-4.

Batchelor G.K., 1953. *The theory of homogenous turbulence*. Cambridge University Press, Cambridge, England.

Batchelor G.K., 1976. Brownian diffusion of particles with hydrodynamic interaction. *J. Fluid Mech.*, 74, 1–29. DOI: 10.1017/S0022112076001663.

Batchelor G.K., 1980. Mass transfer from small particles suspended in turbulent fluid. *J. Fluid Mech.*, 98, 609–623. DOI: 10.1017/S0022112080000304.

Batchelor G.K., Green J.T., 1972. The hydrodynamic interaction of two small freely-moving spheres in linear flow field. *J. Fluid Mech.*, 56, 375–400. DOI: 10.1017/S0022112072002927.

Camp T.R., Stein P.C., 1943. Velocity gradients and internal work in fluid motion. *J. Boston Soc. Civ. Eng.*, 30, 219–237.

Derjaguin B.V., Landau L.D., 1941. Theory of the stability of strongly charged lyophobic sols and of the adhesion of strongly charged particles in solutions of electrolytes. *Acta Physicochim URSS*, 14, 633–660.

Fuchs N., 1934. Über die Stabilität und Aufladung der Aerosole. *Z. Physik*, 89, 736–743. DOI: 10.1007/BF01341386.

Hamaker H.C., 1937. The London–van der Waals attraction between spherical particles. *Physica*, 4, 1058–1072. DOI: 10.1016/S0031-8914(37)80203-7.

Hogg R., Healy T., Fürstenau D.W., 1966. Mutual coagulation of colloidal dispersions. *Trans. Faraday Soc.*, 62, 1638–1651. DOI: 10.1039/tf9666201638.

Hulburt H.M., Katz S., 1964. Some problems in particle technology: A statistical mechanical formulation. *Chem. Eng. Sci.*, 19, 555–574. DOI: 10.1016/0009-2509(64)85047-8.

Lattuada M., Morbidelli M., 2011. Effect of repulsive interactions on the rate of doublet formation of colloidal nanoparticles in the presence of convective transport. *J. Colloid Int. Sci.*, 355, 42–53. DOI: 10.1016/j.jcis.2010.11.070.

Lazzari S., Nicoud L., Jaquet B., Lattuada M., Morbidelli M., 2016. Fractal-like structures in colloid science. *Adv. Colloid Interface Sci.*, 235, 1–13. DOI: 10.1016/j.cis.2016.05.002.

Melis S., Verduyn M., Storti G., Morbidelli M., Bałdyga J., 1999. Effect of fluid motion on the aggregation of small particles subject to interaction forces. *AIChE J.*, 45, 1383–1393. DOI: 10.1002/aic.690450703.

Nicoud L., Lattuada M., Lazzari S., Morbidelli M., 2015. Viscosity scaling in concentrated dispersions and its impact on colloidal aggregation. *Phys. Chem. Chem. Phys.*, 17, 24392–24402. DOI: 10.1039/c5cp03942h.

Saffman P.G., Turner J.S., 1956. On collision of drops in turbulent clouds. *J. Fluid Mech*, 1, 16–30. DOI: 10.1017/S0022112056000020.

Smoluchowski M., 1916. Zur Theorie der Zustandsgleichungen. *Ann. Phys.*, 353, 1098–1102. DOI: 10.1002/andp.19163532407.

Smoluchowski M., 1917. Versuch einer mathematischen Teorie der Koagulationskinetik kolloider Lösungen. *Z. Phys. Chem.*, 92U, 129–168. DOI: 10.1515/zpch-1918-9209.

Spielman L.A., 1970. Viscous interactions in Brownian coagulation. *J. Colloid Interface Sci.*, 33, 562–571. DOI: 10.1016/0021-9797(70)90008-1.

Swift D.L., Friedlander S.K., 1964. The coagulation of hydrosols by brownian motion and laminar shear flow. *J. Colloid Sci.*, 19, 621–647. DOI: 10.1016/0095-8522(64)90085-6.

van de Ven T.G.M., Mason S.G., 1976. The microrheology of colloidal dispersions: IV. Pairs of interacting spheres in shear flow. *J. Colloid Interface Sci.*, 57, 505–516. DOI: 10.1016/0021-9797(76)90229-0.

Verwey E.J.W., Overbeek J.T.G., 1948. *Theory of the stability of lyophobic colloids*. Elsevier, Amsterdam, Netherlands.

Zaccone A., Wu H., Gentili D., Morbidelli M., 2009. Theory of activated-rate processes under shear with application to shear-induced aggregation of colloids. *Phys. Rev. E*, 80, 051404. DOI: 10.1103/PhysRevE.80.051404.

Zeichner G.R., Schowalter W.R., 1977. Use of trajectory analysis to study stability of colloidal dispersions in flow fields. *AIChE J.*, 23, 243–254. DOI: 10.1002/aic.690230306.

Zinchenko A.Z., Davis R.H., 1995. Collision rates of spherical drops of particles in a shear flow at arbitrary Peclet numbers. *Phys. Fluids*, 7, 2310–2327. DOI: 10.1063/1.868745.

APPENDIX

A comprehensive guide for choosing the values of parameters α and c_2 has been presented in the supplementary material to the paper by Lattuada and Morbidelli (2011). In the case of parameter α, a simple size-dependent correlation was presented for an extensional flow that reads as follows:

$$\alpha = \frac{4}{3\sqrt{3}} \cdot 0.4 \left(\frac{a_i}{a_{\text{ref}}} \right)^{-0.26} \tag{A1}$$

where a_{ref} is a reference particle radius and equals 50 nm. For particle radius $a_i = 100$ nm we can easily calculate $\alpha = 0.257$.

A similar correlation has not been provided for the simple shear flow. However, in the course of this study it has been found that for particle radius of 100 nm, the best agreement between the simplified kernel and the full solution can be obtained for $\alpha = 0.11$. This value remains constant for all simulations with $a_i = 100$ nm.

Parameter c_2 has been estimated based on the data presented in the supplementary material to Lattuada and Morbidelli (2011) with the initial guess of its value assumed in a way to match c_2 constant in similar systems. Moreover, parameter c_2 was found to be independent of the type of flow pattern. The final set of all parameters used for Model II is presented in Table A1.

Table A1. Set of parameters used for Model II

a_i [nm]	Rp [–]	κa [–]	α	c_2	Flow pattern
100	0.27	33	0.11	1	Shear
100	2.39	33	0.11	4.5	Shear
100	2.39	4.7	0.11	1.7	Shear
100	0.27	33	0.257	1	Extensional
100	2.39	33	0.257	4.5	Extensional
100	2.39	4.7	0.257	1.7	Extensional

Received 07 June 2021
Received in revised form 21 August 2021
Accepted 01 September 2021